Heliostat Aerodynamics and Wind Load: Measurements, Characterization and Prediction in Atmospheric Boundary Layer

Matthew Emes
The University of Adelaide

HelioCon Seminar
13 July 2022

ASTRI
Australian Solar Thermal Research Institute

Heliostat aerodynamics research

Prof Maziar Arjomandi 2014-2022

- Research Director, Mechanical Engineering
- Leading ASTRI heliostat project

Dr Matthew Emes 2014-2022

- Postdoctoral Research Associate
- Co-leading ASTRI heliostat project, ABLRF manager

Dr Azadeh Jafari 2017-2022

- Postdoctoral Research Associate
- Turbulent boundary layer analysis and control

PhD students

- Sahar Bakhshipour
- Matthew Marano

Motivation

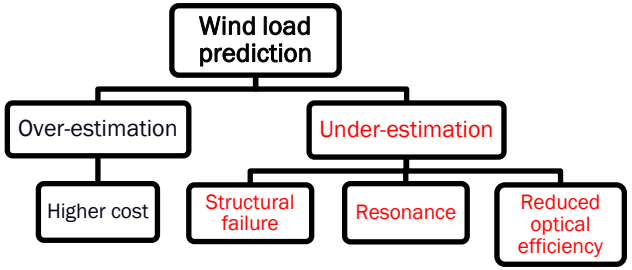

- Heliostat cost reduced by 40% by lowering the stow design wind speed from 20 m/s to 10 m/s*
- Increasing turbulence in a high-roughness terrain results in 10% increase in cost of a 25 m^2 heliostat and 13% increase in cost of a 150 m^2 heliostat**

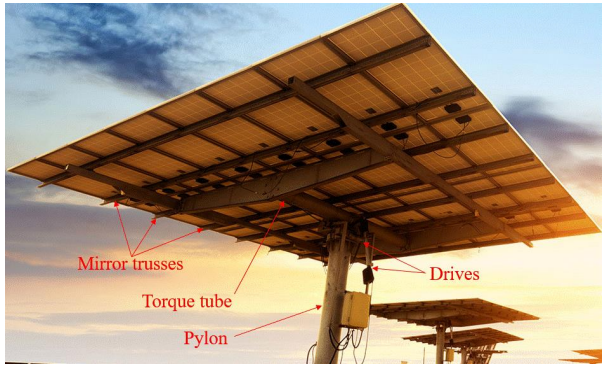

Abengoa Solar heliostat (Advisian Worley Group 2021)

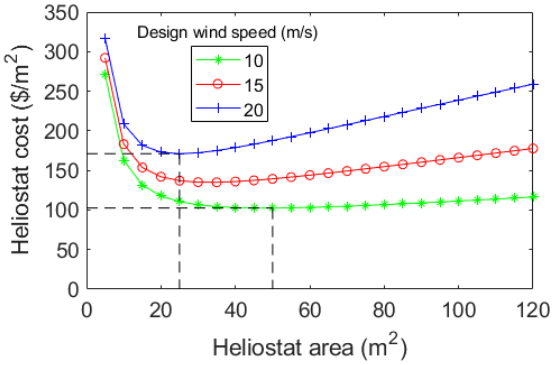

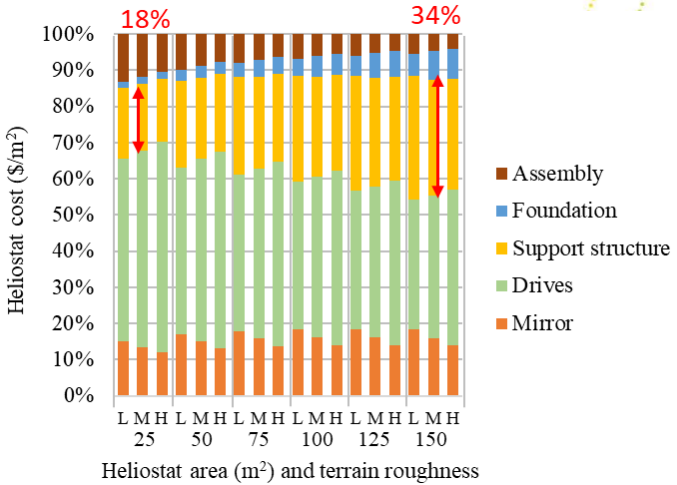

*Emes *et al.* (2015), Effect of heliostat design wind speed on the levelised cost of electricity from concentrating solar thermal power tower plants, *Solar Energy*
**Emes *et al.* (2020), The influence of atmospheric boundary layer turbulence on the design wind loads and cost of heliostats, *Solar Energy*

University of Adelaide wind tunnel

Atmospheric test section

- 3 m × 3 m cross-section and 17 m development length
- 33 m/s (120 km/h) maximum flow speed
- Base force balance containing six-axis load cell
- Electronic turntable for azimuth angle adjustment
- 2D traverse for flow mapping
- Sets of spires and roughness elements for generation of ABL with different surface roughness and turbulence characteristics
- Heliostat models with differential pressure sensors and load cells

$Re_\infty = U_\infty \delta/\nu \approx 8.8\times10^5$ δ = 1-2 m

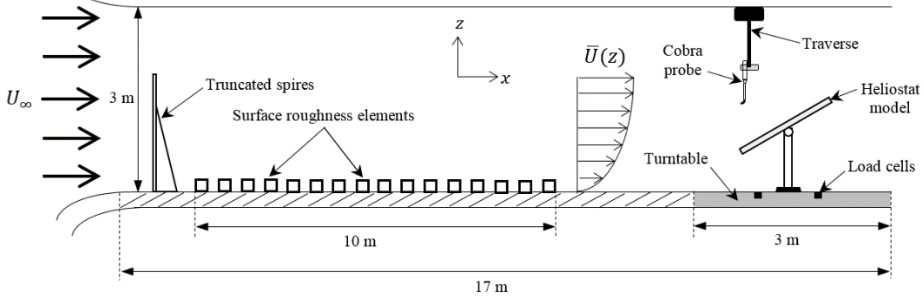

Arjomandi *et al.* (2020), A summary of experimental studies on heliostat wind loads in a turbulent atmospheric boundary layer, AIP Conference Proceedings, *SolarPACES*

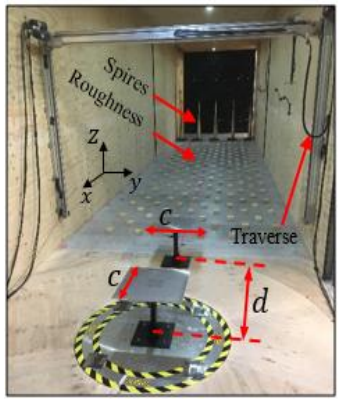

d/c = 2-8

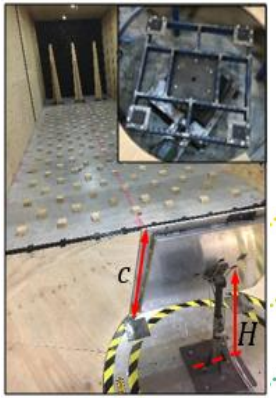

c = 0.2-0.8 m
H = 0.15-0.5 m

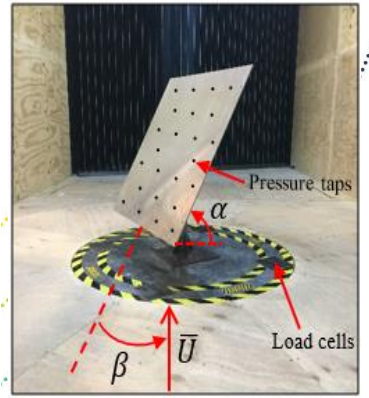

α = 0-90°
β = 0-180°

Wind tunnel flow aerodynamics instrumentation

- Multi-hole pressure “Cobra” probes (Turbulent Flow Instrumentation)
  - Three velocity components (u, v, w) accuracy ±0.5 m/s, ±1.0° pitch and yaw angles
  - Flow speeds up to 60 m/s at 1 kHz sampling frequency
- 6-axis load cell (JR3)
  - Fx, Fy ±100N, Fz ±200N, Mx, My, Mz ±12 Nm, accuracy ±0.25%
- Three-axis load cells (Bestech)
  - 2 N, 10 N, 100 N, 500 N
- Differential pressure sensors (Honeywell)
  - Pressure range of ±250Pa
  - Accuracy of ±0.25%

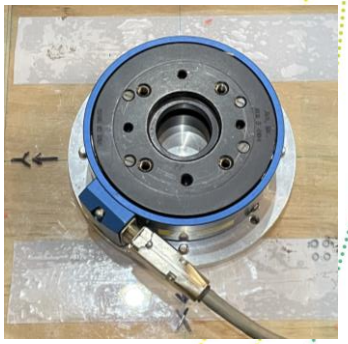

Atmospheric boundary layer (ABL) turbulence

- Longitudinal (I_u, L_u^x) and vertical (I_w, L_w^x) turbulence dependent on height, surface roughness* and atmospheric stability**

Terrain roughness	z_0(m)	α_U	I_u (z)	I_u(%) at z= 10 m
Low (LR)	0.003	0.12	–1.7 (ln$z$)+ 17.2	13.3
Medium (MR)	0.03	0.17	–2.3 (ln$z$)+ 23.1	17.8
High (HR)	0.3	0.22	–4.4 (ln$z$)+ 38.9	28.8

*Emes *et al.* (2020), The influence of atmospheric boundary layer turbulence on the design wind loads and cost of heliostats, *Solar Energy*
**Emes *et al.* (2019), Turbulence length scales in a low-roughness near-neutral atmospheric surface layer, *Turbulence*

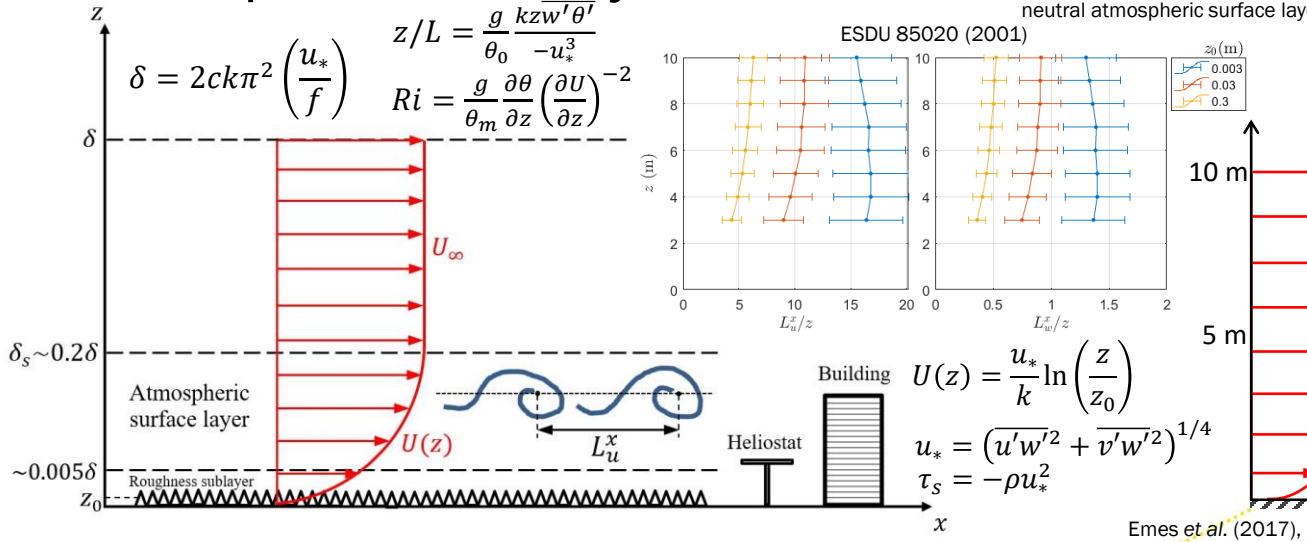

$$U(z) = \frac{u_*}{k}\ln\left(\frac{z}{z_0}\right)$$

$$u_* = \left(\overline{u'w'}^2 + \overline{v'w'}^2\right)^{1/4}$$

$$\tau_s = -\rho u_*^2$$

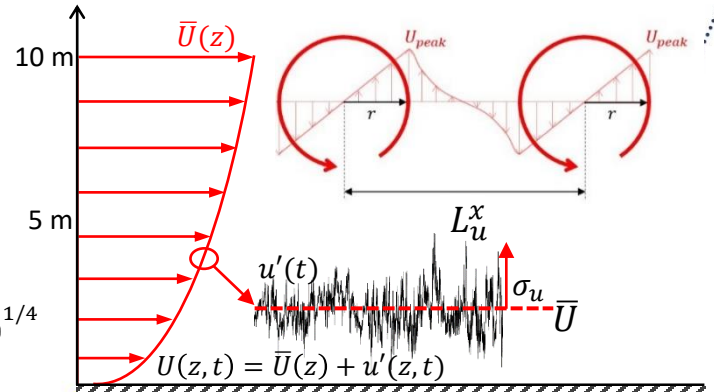

Emes *et al.* (2017), Effect of turbulence characteristics in the atmospheric surface layer on the peak wind loads on heliostats in stow position, *Solar Energy*

Heliostat wind load coefficients

$$C_{Fx} = \frac{F_x}{1/2\rho \bar{U}_H{}^2 A}$$

$$C_{Fz} = \frac{F_z}{1/2\rho \bar{U}_H{}^2 A}$$

$$C_{MHy} = \frac{M_{Hy}}{1/2\rho \bar{U}_H{}^2 Ac}$$

$$C_{My} = C_{MHy}\left(\frac{c}{H}\right) + C_{Fx}$$

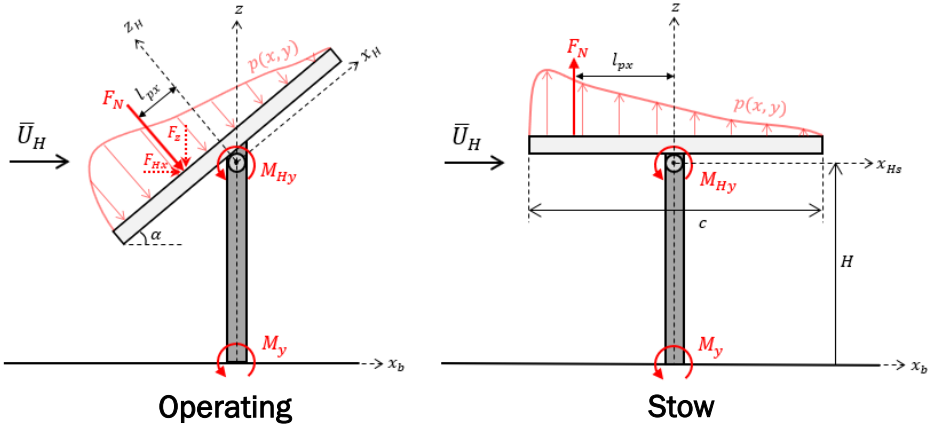

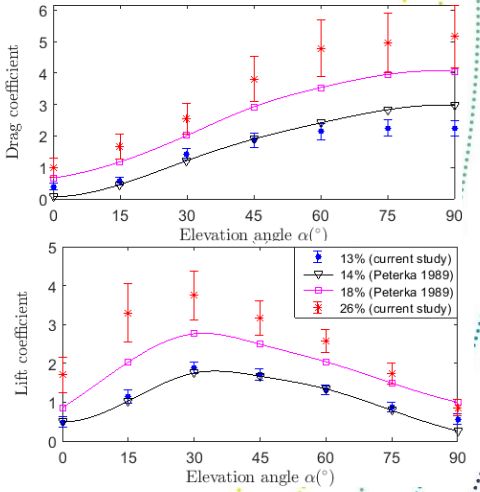

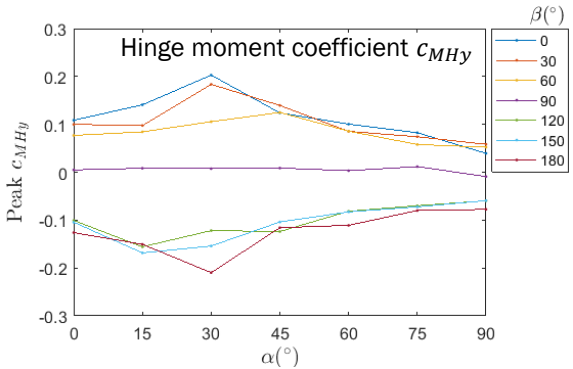

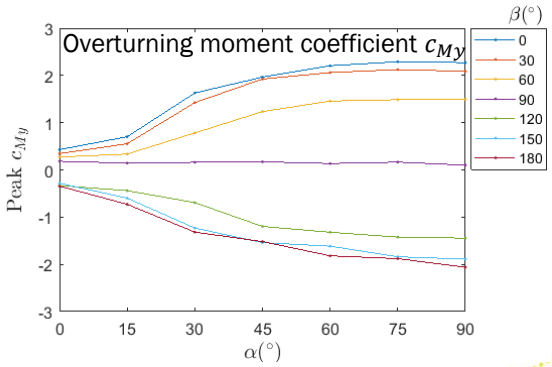

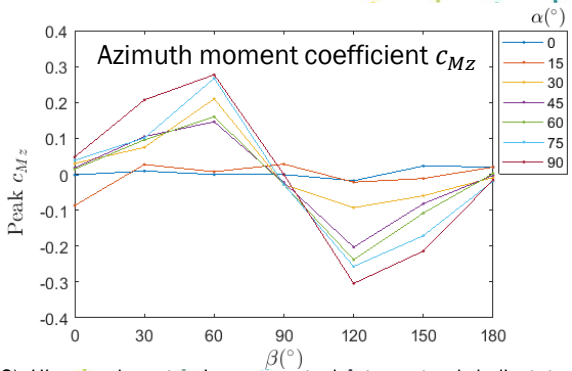

Emes *et al.* (2019), Hinge and overturning moments due to unsteady heliostat pressure distributions in a turbulent atmospheric boundary layer, *Solar Energy*

Heliostat wind load turbulence correlations

- Correlation of turbulence intensities and length scales with peak drag and lift coefficients*
- Effect of stow height on peak lift coefficient*,**

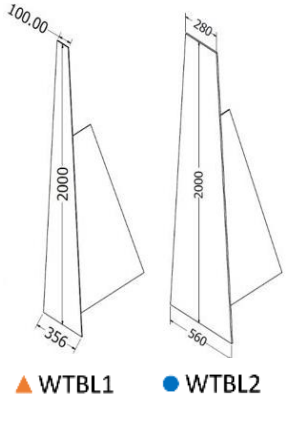

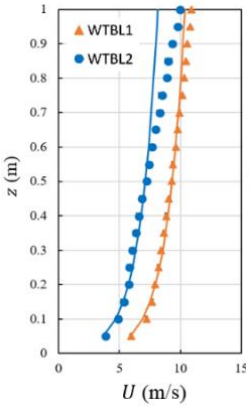

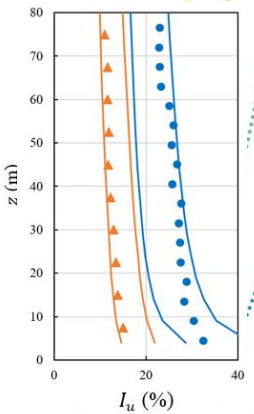

*Jafari *et al.* (2019), Correlating turbulence intensity and length scale with the unsteady lift force on flat plates in an atmospheric boundary layer flow, *JWEIA*

**Emes *et al.* (2017), Effect of turbulence characteristics in the atmospheric surface layer on the peak wind loads on heliostats in stow position, *Solar Energy*

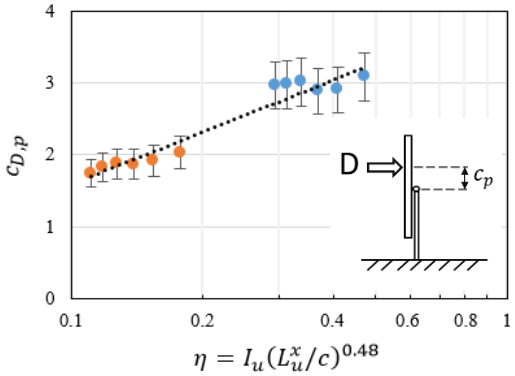

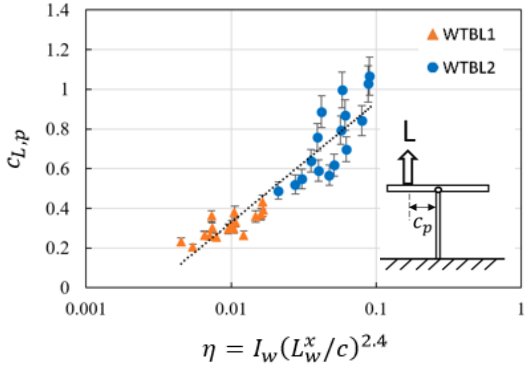

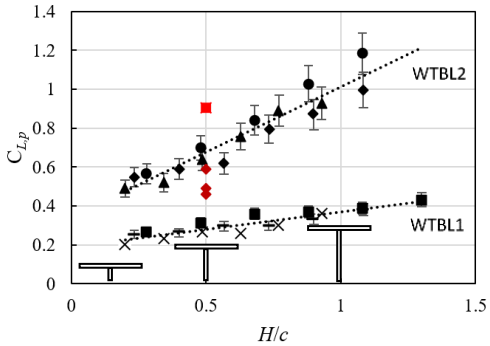

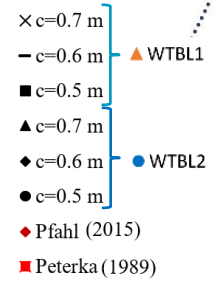

Wind tunnel scaling of turbulence spectra

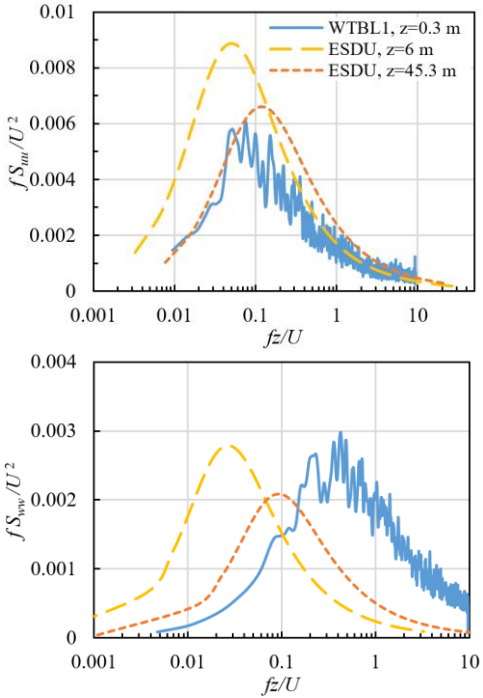

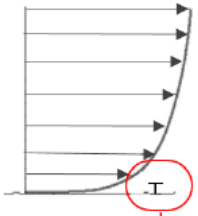

$$|A_i(f)|^2 = \frac{U^2 S_{c_i}(f)}{C_i^2 \, S_{jj}(f)}$$

$i = L$ (lift), D(drag)
$j = u, w$

Full scale

Model scale

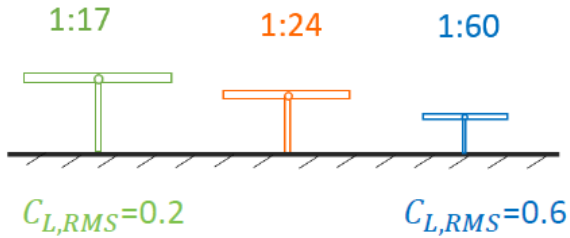

Restricted generation of vertical turbulence in wind tunnel (1:60 horizontal, 1:24 vertical)

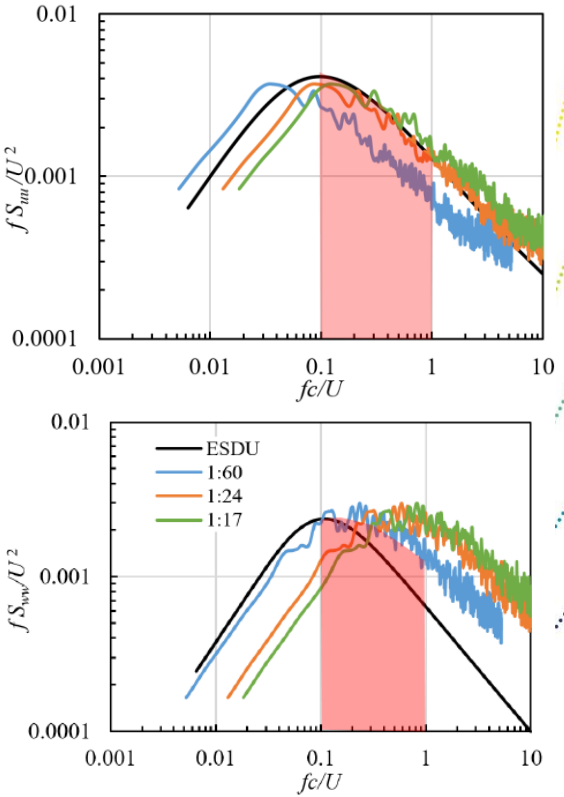

Jafari *et al.* (2019), Measurement of unsteady wind loads in a wind tunnel: scaling of turbulence spectra, *JWEIA*

Centre of pressure distributions

$$F_N(t) = 1/2\rho\bar{U}_H{}^2 \oint -C_{P_i}(t)\, dA \qquad C_{P_i}(t) = \frac{p'(t)}{1/2\rho\bar{U}_H{}^2}$$

$$F_x(t) = F_N(t)\sin\alpha$$

$$F_z(t) = F_N(t)\cos\alpha$$

$$l_{px}(t) = \frac{c}{2} - \frac{\int_0^c xp'(t,x,y)dx}{\int_0^c p'(t,x,y)dx}$$

$$M_{Hy}(t) = F_N(t)l_{px}(t)$$

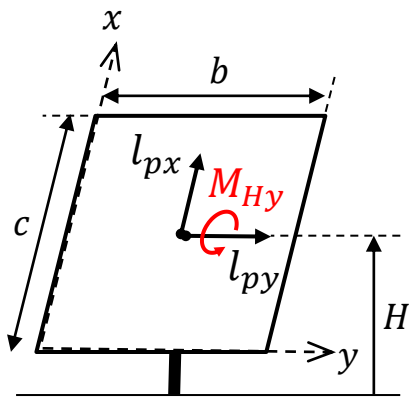

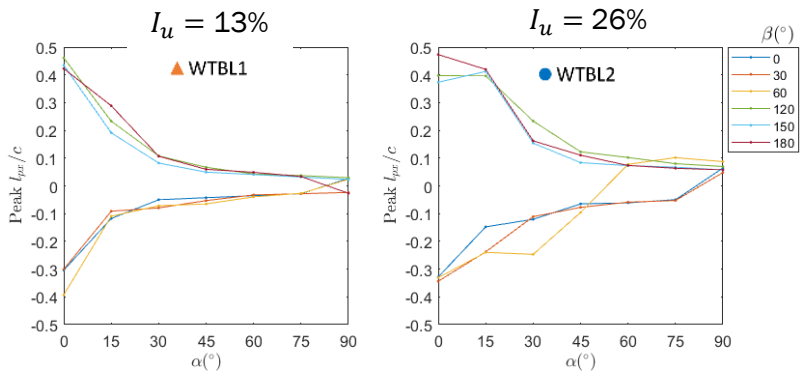

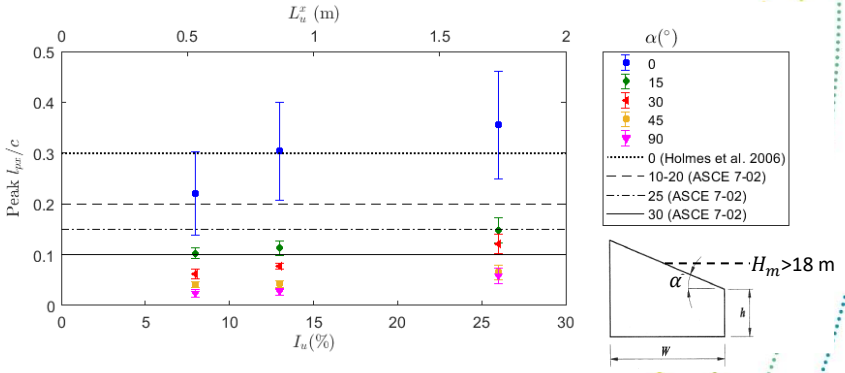

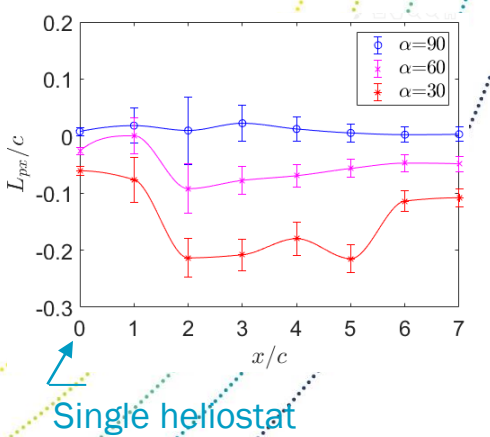

Single heliostat

Emes *et al.* (2019), Hinge and overturning moments due to unsteady heliostat pressure distributions in a turbulent atmospheric boundary layer, *Solar Energy*

Wind load design guidelines

- ASCE/SEI 7-16

$$p = q_h(GC_p)\gamma_E\gamma_a$$

  Chapter 29.4.4 Rooftop Solar Panels Parallel to the Roof Surface on Buildings of All Heights and Roof Slopes
  - **Rooftop solar panels** tilted on flat roof
  - Rooftop panels parallel to angled roof
  - Array edge factor ($1.0 \leq \gamma_E \leq 1.5$) and panel pressure equalization factor ($0.4 \leq \gamma_a \leq 0.8$)
- IEC 61400-1

  Wind turbines – design requirements
  - Guidelines for **wind turbine** classes (turbulence conditions), extreme operating gust, load calculations across rotor plane

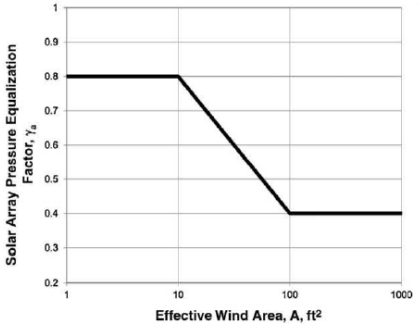

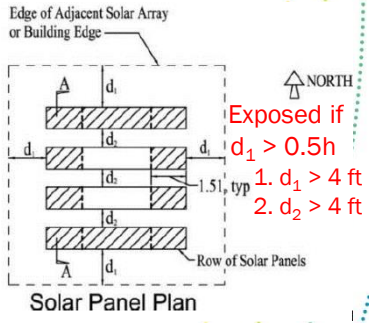

Kopp *et al.* (2012), Aerodynamic mechanisms for wind loads on tilted, roof-mounted, solar arrays, *JWEIA*
Stenabaugh *et al.* (2015), Wind loads on photovoltaic arrays mounted on sloped roofs of low-rise building parallel to the roof surface, *JWEIA*

Murphy (1980), Wind loading on tracking and field-mounted solar collectors, SERI-TP-632-958

Collector Technology	Heliostats[a]
Maximum survival wind speed, m/s(mph)	(stowed) 40 (90)
Design wind speed for normal operation, m/s (mph)	12 (27)
Maximum wind speed during which collector must track, m/s(mph)	22 (50)
Stated or implied mean recurrence internal, yr	100 (extreme)

ASTRI heliostat wind load spreadsheet

- Publicly available heliostat wind load calculator (version 1c) https://www.adelaide.edu.au/cet/technologies/heliostat-wind-loads#research-data
- Heliostat design (maximum) wind loads calculated based on:
  1) Full-scale heliostat characteristic dimensions and design wind speeds
  2) Dependence of wind load coefficients in UoA wind tunnel experiments

	Operating loads ($\alpha > 0°$)							Stow loads ($\alpha = 0°$)					
WTBL1													
(I_u=13%)	**α (°)**	**β (°)**	**cFx**	**cFz**	**cMHy**	**cMy**	**cMz**	**β (°)**	**cFx**	**cFz**	**cMHy**	**cMy**	**cMz**
Fx max	75	0	2.25	0.88	0.08	2.29	0.06	0	0.39	0.49	0.11	0.43	0.00
Fz max	30	0	1.42	1.89	0.20	1.63	0.04	0	0.39	0.49	0.11	0.43	0.00
MHy max	30	180	-1.12	-1.51	-0.21	-1.32	-0.01	180	-0.32	-0.48	-0.13	-0.34	0.03
My max	75	0	2.25	0.88	0.08	2.29	0.06	0	0.39	0.49	0.11	0.43	0.00
Mz max	75	120	-1.38	-0.60	-0.07	-1.42	-0.50	150	-0.27	-0.46	-0.10	0.43	0.03
WTBL2													
(I_u=26%)	**α (°)**	**β (°)**	**cFx**	**cFz**	**cMHy**	**cMy**	**cMz**	**β (°)**	**cFx**	**cFz**	**cMHy**	**cMy**	**cMz**
Fx max	90	0	5.16	0.86	0.21	5.33	0.12	90	1.10	1.64	-0.01	-0.55	0.05
Fz max	30	0	2.55	3.74	0.65	3.11	0.68	60	1.06	1.96	0.40	1.10	0.05
MHy max	15	180	-1.56	-2.15	-0.76	-2.03	-0.05	0	1.00	1.70	0.45	1.18	0.00
My max	90	0	5.16	0.86	0.21	5.33	0.68	0	1.00	1.70	0.45	1.18	0.00
Mz max	90	60	2.52	1.19	-0.45	2.65	1.36	150	-0.78	-0.88	-0.10	-0.80	0.07

Heliostat wind load design guidelines

SolarPACES Task III meeting (2019-), draft document version 4

1. Dimensions of the azimuth-elevation heliostat: mirror chord length (and width), elevation axis (hinge) height
2. Compute the effective heliostat mirror area
3. Determine the design (gust and mean) wind speeds at the elevation axis height of the heliostat, based on historical wind data measured at the site of the heliostat field. In the absence of historical wind data, approximate the wind profiles of the terrain surrounding the heliostat field from the estimated surface roughness height or using local wind maps in the design actions for physical structures in relevant wind load design codes and standards
4. Determine the turbulence intensity from the design wind speeds in step 3 for two heliostat load cases: (1) operation, (2) stow
5. Determine the mean and peak load coefficients from the pressure and load distributions corresponding to the maximum operating and stow cases, adopting the following wind tunnel design practices:
   - Scale models of 1:20 to 1:50 with smaller scaling ratios necessary to reproduce the vertical turbulence spectrum for loads in stow position
   - Test elevation angles in increments of 30°, with operating loads in the 30-60° range in 5° increments
   - Test azimuth angles in increments of 10-30°
   - Force balance load cells and pressure sensors

Heliostat wind load design guidelines

SolarPACES Task III meeting (2019-), draft document version 4

6. Calculate the design loads based on global and local wind effects on the heliostat using peak coefficients and appropriate load-response correlations for the relevant design wind speeds from the analysis of wind data
   - Global wind effects should consider the bending moment reactions on the heliostat to be resisted by the drives, torque tube and foundation
   - Local wind effects should consider the reactions of local connections, beams and truss elements resulting from the global effects, such as torsional rotation of the pylon and deformations of the mirror surface
7. Apply aspect ratio adjustment factor for non-square heliostats e.g. Pfahl *et al.* (2011)
8. Consider safety factors for alternative heliostat designs to a conventional azimuth-elevation tracking configuration (e.g. spinning axis, tilt-roll)
   - Resonance effects in the transition to stow due to increases of wind speed at intermediate operating angles
   - Lowering of the mirror closer to the ground in stow position

https://www.adelaide.edu.au/cet/technologies/heliostat-wind-loads#research-data

Dynamic wind load analysis

- Fluctuating spectral characteristics of the maximum loading cases for the elevation drive, azimuth drive and pedestal
  - Maximum hinge moment due to unsteady pressure distribution and movement of the centre of pressure towards the leading edge*
  - Gaussian load distribution for low to moderate turbulence (I_u = 10-15%) generated in the wind tunnel**
- Challenges in wind tunnel scaling of structural properties of heliostat
- Need for field-scale investigations to better understand dynamic loads and wind-induced displacements due to heliostat field interactions

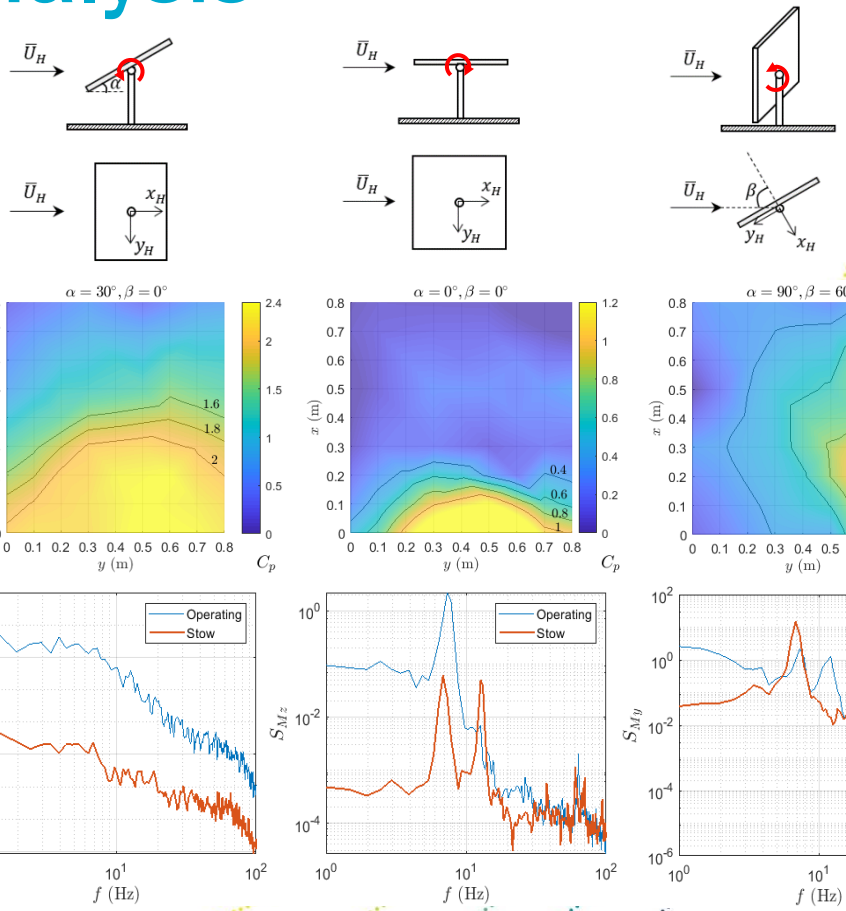

*Emes *et al.* (2019), Hinge and overturning moments due to unsteady heliostat pressure distributions in a turbulent atmospheric boundary layer, *Solar Energy*

**Emes *et al.* (2020), Wind load design considerations for the elevation and azimuth drives of a heliostat, AIP Conference Proceedings, *SolarPACES*

Pedestal stress distributions in ABL

$$\sigma_{c,ped} = \sqrt{\sigma_{b,ped}^2 + 3\sigma_{t,ped}^2} \quad \{\text{von Mises}\}$$

$$\sigma_{b1} = \frac{32 M_y D_{ped}}{\pi(D_{ped}^4 - d_{ped}^4)}$$

$$\sigma_{b2} = \frac{32 x \sin\alpha\, F_g D_{ped}}{\pi(D_{ped}^4 - d_{ped}^4)}$$

$$\sigma_{b3} = \frac{4 F_g}{\pi(D_{ped}^2 - d_{ped}^2)}$$

$$\sigma_{t,ped} = \frac{16 M_z D_{ped}}{\pi(D_{ped}^4 - d_{ped}^4)}$$

Terrain roughness	z_0(m)	α_U	I_u (z)	I_u(%) at z= 10 m
Low (LR)	0.003	0.12	–1.7 (ln$z$)+ 17.2	13.3
Medium (MR)	0.03	0.17	–2.3 (ln$z$)+ 23.1	17.8
High (HR)	0.3	0.22	–4.4 (ln$z$)+ 38.9	28.8

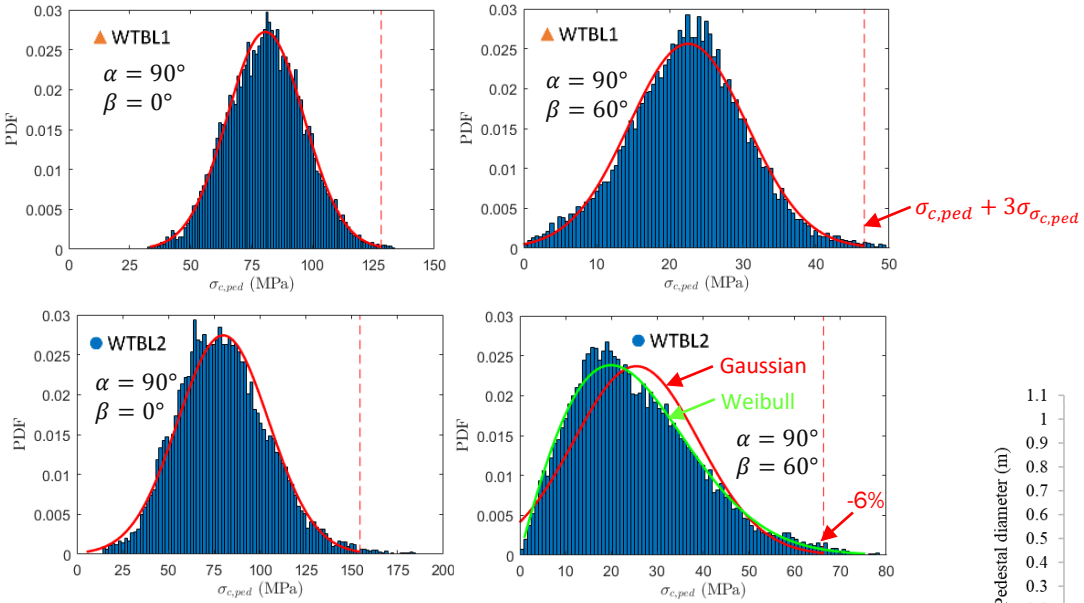

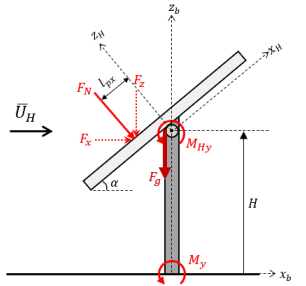

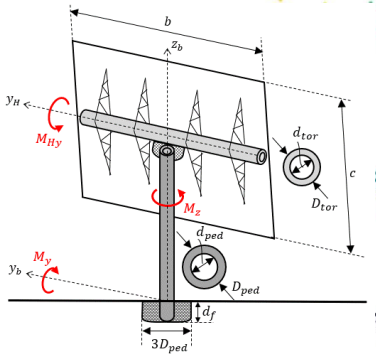

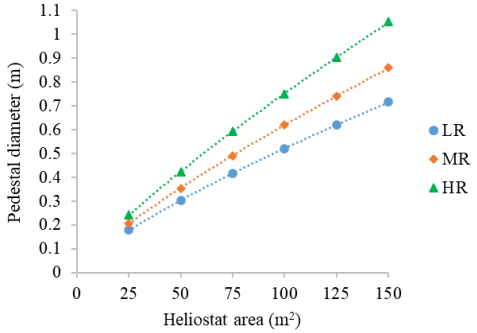

Emes *et al.* (2020), The influence of atmospheric boundary layer turbulence on the design wind loads and cost of heliostats, *Solar Energy*

Torque tube stress distributions in ABL

$$\sigma_{c,tor} = \sqrt{\sigma_{b,tor}^2 + 3\sigma_{t,tor}^2} \quad \{\text{von Mises}\}$$

$$\sigma_{b,tor} = \frac{4D_{tor}c\sqrt{F_x^2 + (F_z - F_g)^2}}{\pi(D_{tor}^4 - d_{tor}^4)}$$

$$\sigma_{t,tor} = \frac{16M_{Hy}D_{tor}}{\pi(D_{tor}^4 - d_{tor}^4)}$$

Terrain roughness	z_0(m)	α_U	I_u (z)	I_u(%) at z= 10 m
Low (LR)	0.003	0.12	–1.7 (lnz)+ 17.2	13.3
Medium (MR)	0.03	0.17	–2.3 (lnz)+ 23.1	17.8
High (HR)	0.3	0.22	–4.4 (lnz)+ 38.9	28.8

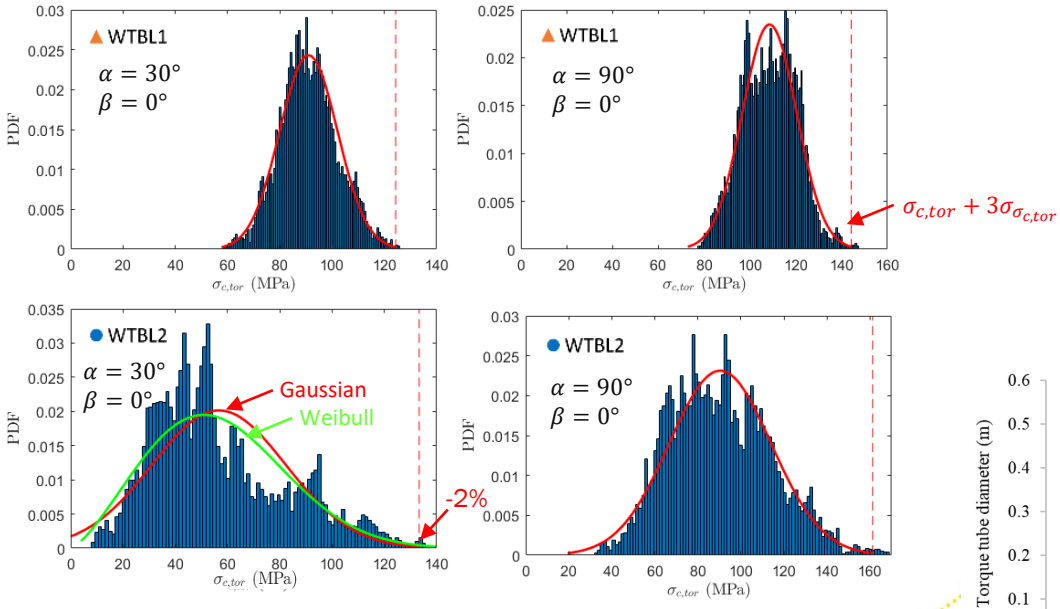

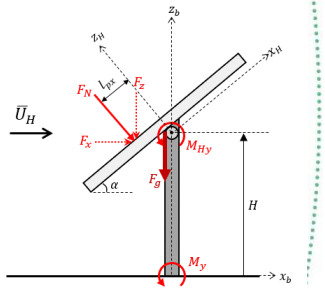

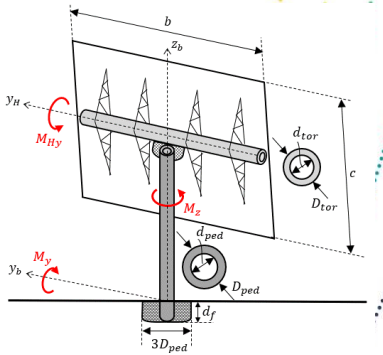

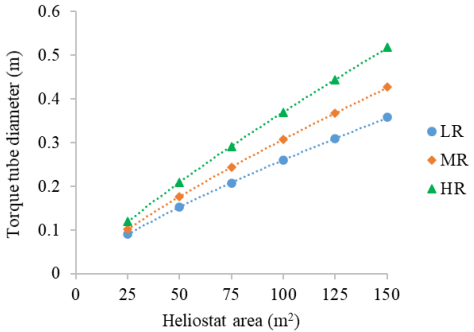

Emes *et al.* (2020), The influence of atmospheric boundary layer turbulence on the design wind loads and cost of heliostats, *Solar Energy*

Heliostat field stow strategy for wind

- Statistical correlation of DNI, tracking angles and CSAT3 wind data at PSA CESA-I field of 300 heliostats
- Annual field operation increased by 6% with increasing stow design wind speed from 6 m/s to 12 m/s
- Annual thermal energy capture increased by 1.2% with $\beta = 90 \pm 15°$ stowing strategy at wind speeds exceeding 10 m/s

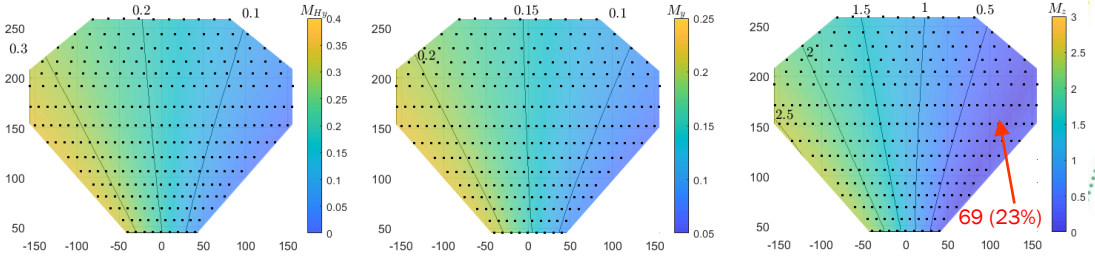

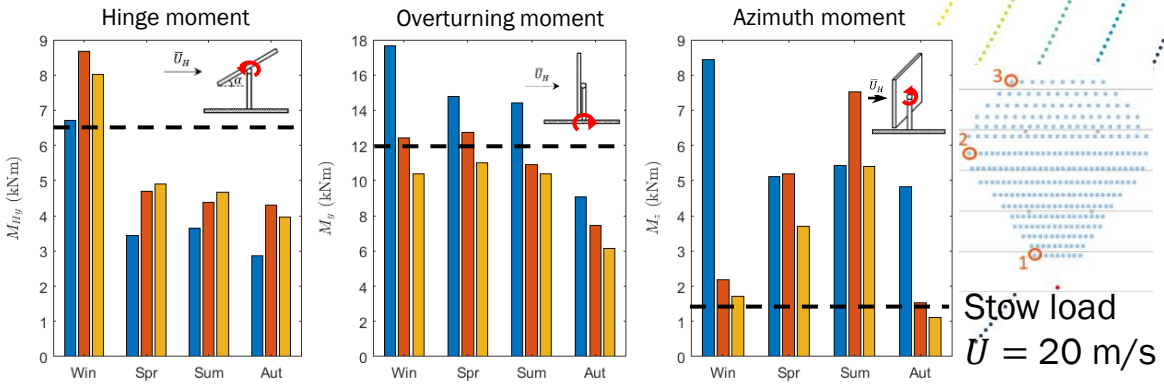

Emes *et al.* (2022), Stowing Strategy for a Heliostat Field Based on Wind Speed and Direction, AIP Conference Proceedings, *SolarPACES*

Tandem heliostat wind loads

- Peak loads on a second heliostat in tandem configuration are dependent on the spacing between the heliostats*,**
- Unsteady wake generated by upstream heliostat leads to increased turbulence and peak hinge moment at high field densities, e.g. $x/c = 3$*

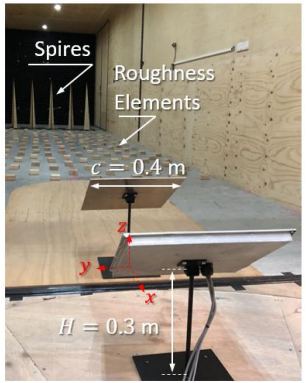

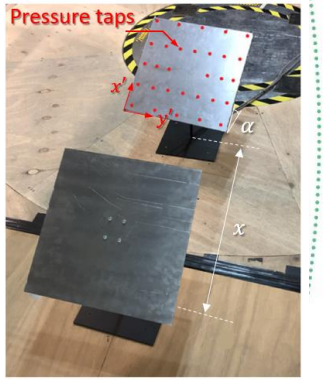

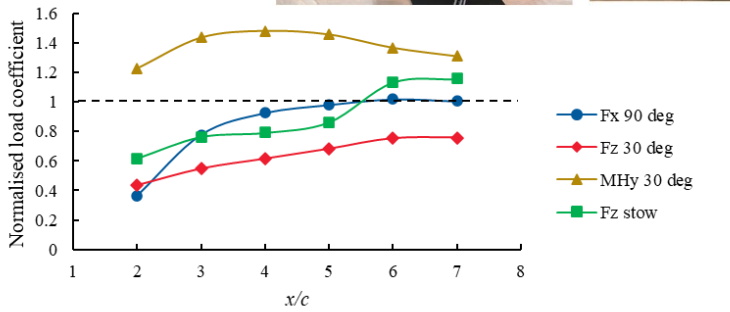

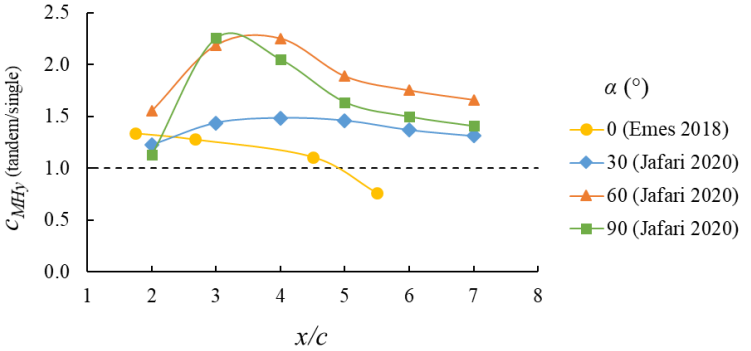

*Jafari *et al.* (2020), An experimental investigation of unsteady pressure distribution on tandem heliostats, AIP Conference Proceedings, *SolarPACES*
**Emes *et al.* (2018), Investigation of peak wind loads on tandem heliostats in stow position, *Renewable Energy*

Mesh grid retrofits for wind load reduction

- Lower fence porosity creates larger wind load reduction up to 50% in drag and 55% in lift
- Turbulence mitigation and wind load reduction for heliostat hinge to fence height < 0.375 (z/H < 0.8 at all α)
- Operating wind load reduction of 15-20% for 0.46 porosity edge-mounted mesh device

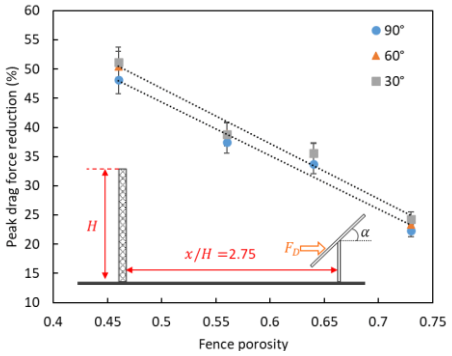

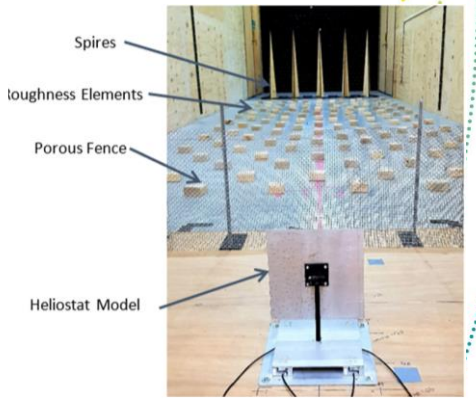

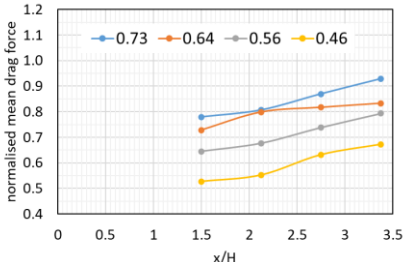

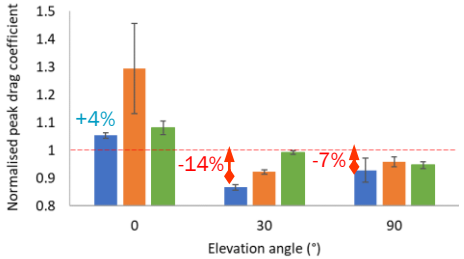

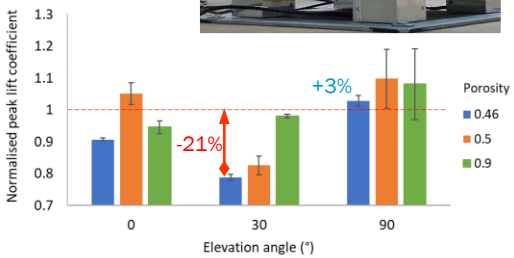

Emes *et al.* (2022), A feasibility study on the application of mesh grids for heliostat wind load reduction, *Solar Energy*

Heliostat shape and field aerodynamics

- Aspect ratio and gap effects on static and dynamic wind loads
- Heliostat field model with 1/16th radial sectors on 2.7 m diameter platform

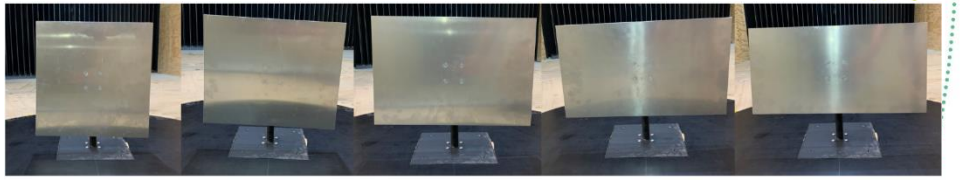

a) AR=1 b) AR=1.25 c) AR=1.5 d) AR=1.75 e) AR=2

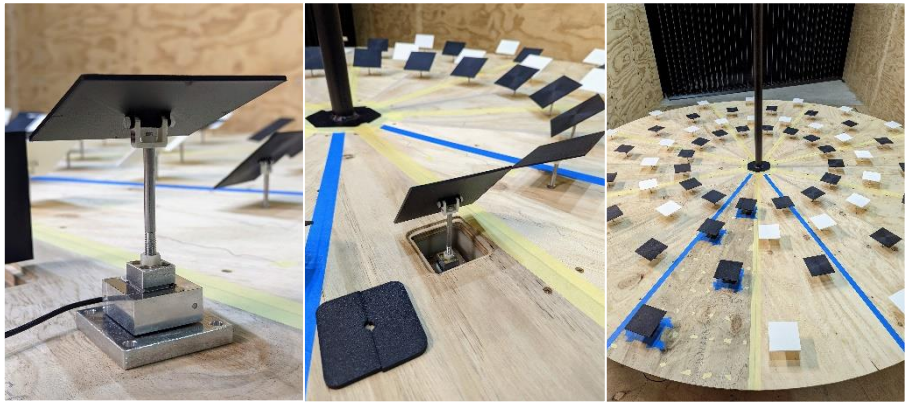

Effect of aspect ratio

- Pfahl et al. (2011) found that all loads (except CMz and stow CFz) decreased with increasing AR from 0.5 to 3 and constant gap ratio (gap/height) = 0.13
- Similar trends observed at UoA with increasing AR – reductions in CFx, CMy and CFz with increasing AR from 1 to 1.5 are 13%, 29% and 10% in Pfahl et al. (2011)
- The results demonstrate the benefit of reducing the pylon height and gap with the ground on maximum wind loads on operating and stowed heliostats

ΔAR	Average gap ratio	ΔCFx (%)	ΔCMy (%)	ΔCFz (%)
1-1.5	0.18	-7	-14	-12
1.25-1.75	0.24	-6	-11	-4
1.25-2	0.29	-11	-12	1
1.5-2	0.34	-9	-8	-3

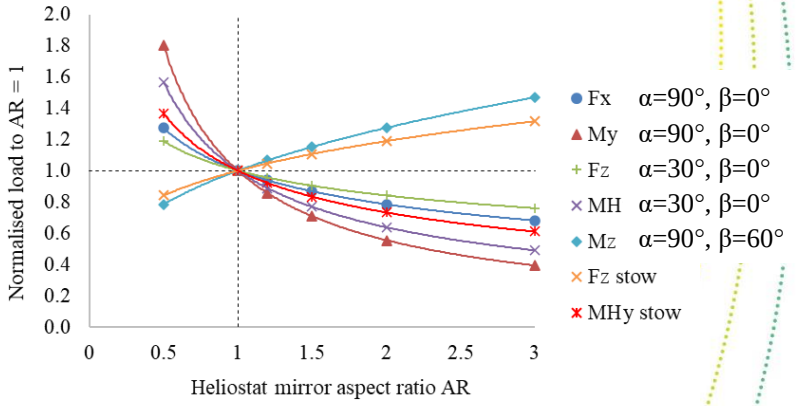

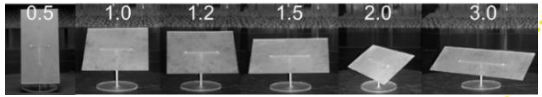

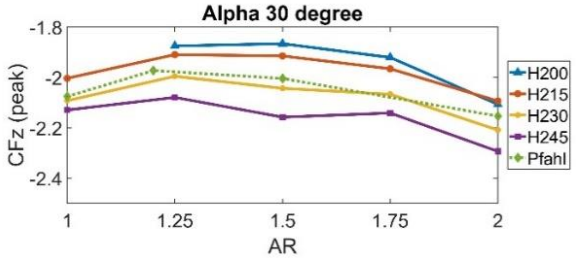

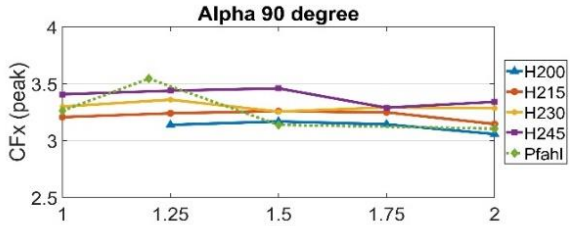

Effect of gap (ground clearance) ratio

- Decreasing CFx and CMy at α = 90° with decreasing gap ratio, relatively independent of aspect ratio
- Decreasing CFz at α = 30° with decreasing gap ratio, with largest reductions at AR ≥ 1.25
- At constant aspect ratio, reductions of 4-9% in peak CFx, 10-17% in peak CMy and 4-13% in peak CFz with maximum reductions in CFx, CMy and CFz at AR = 1.5

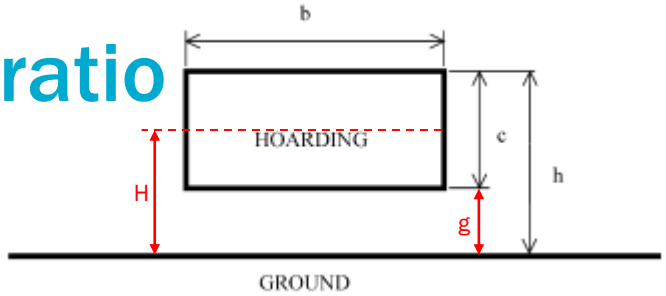

Letchford (2001), Wind loads on rectangular signboards and hoardings, *JWEIA*

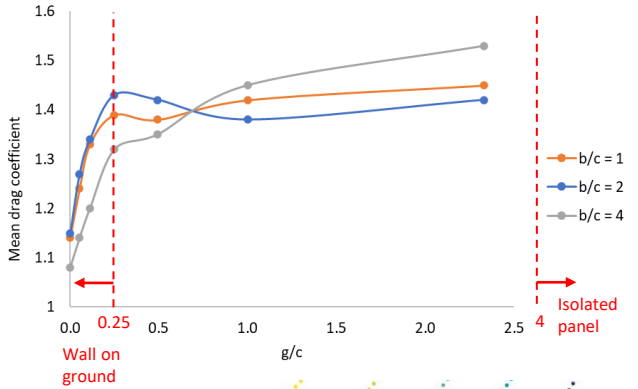

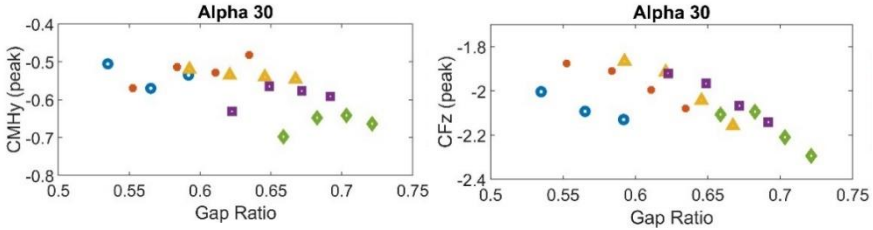

As gap reduced, separating shear layer interaction suppressed and reduced drag

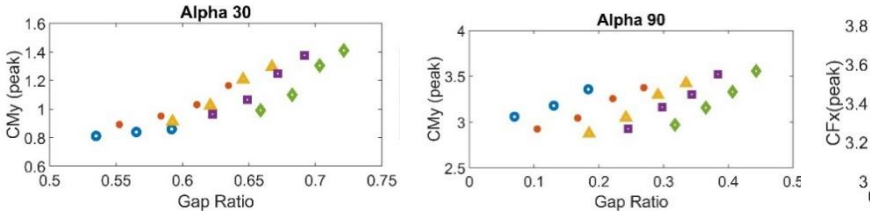

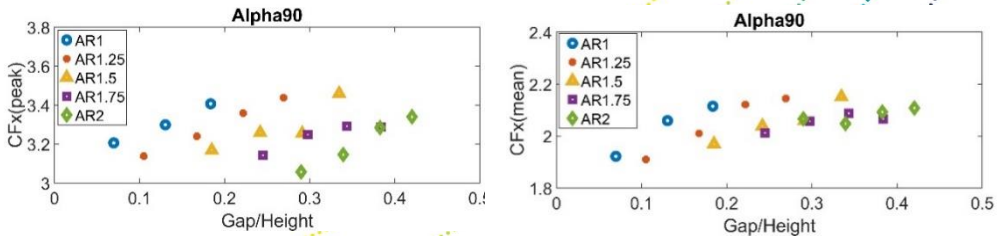

Atmospheric Boundary Layer Research Facility (ABLRF)

- Open farmland on University of Adelaide Roseworthy campus
- Horizontal and vertical arrays of ultrasonic anemometers to characterise 3D turbulence intensities and length scales
- Az-El heliostat (3 m × 2 m) with 48 differential pressure sensors and 6-axis load cell to verify UoA wind tunnel data

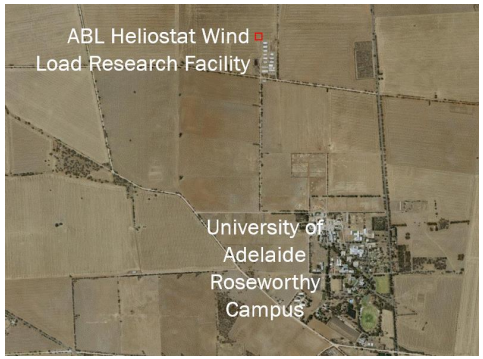

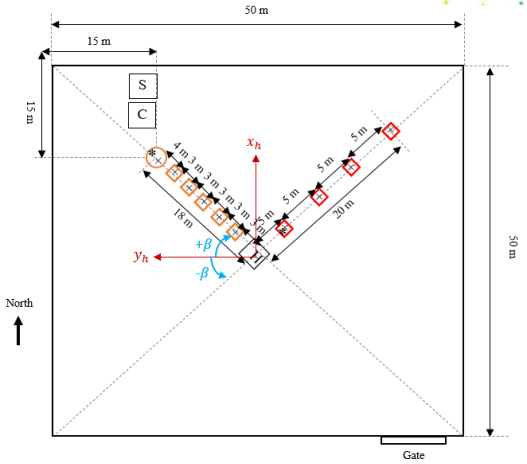

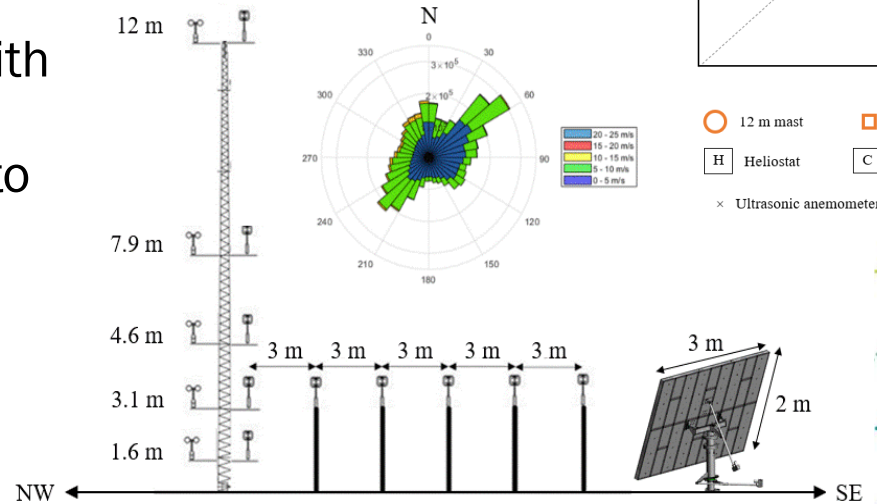

ABLRF instrumentation

- 14 UA to characterise 3D turbulence and thermal stability
- 9 CA to verify mean wind profiles

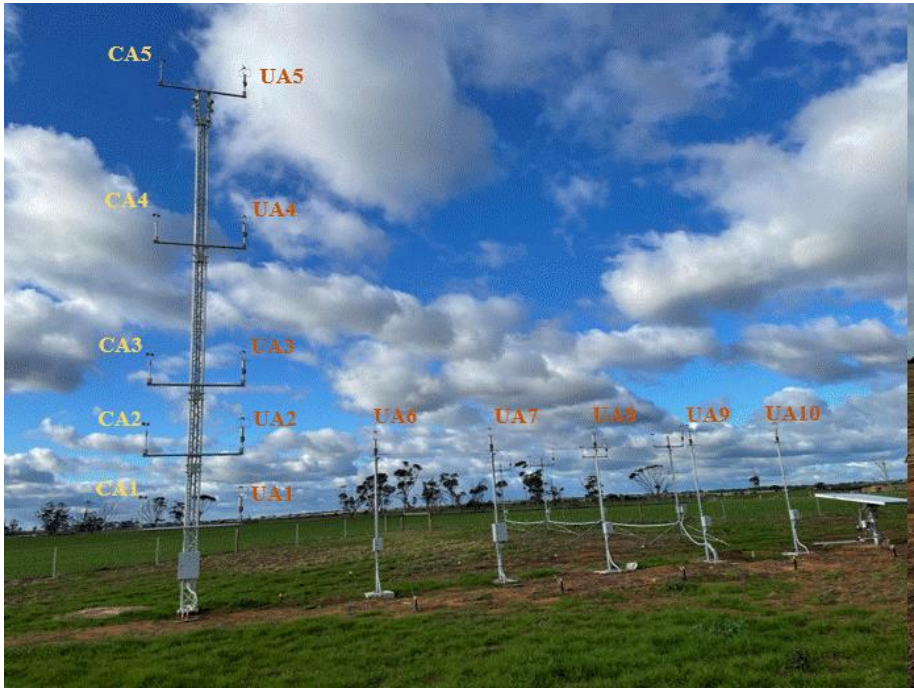

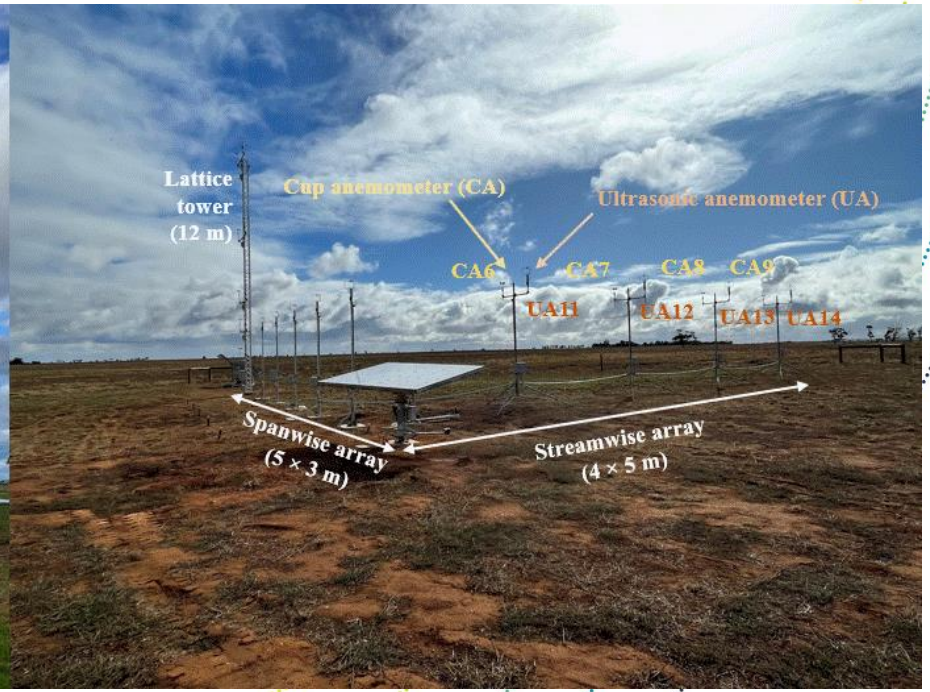

ABLRF preliminary data

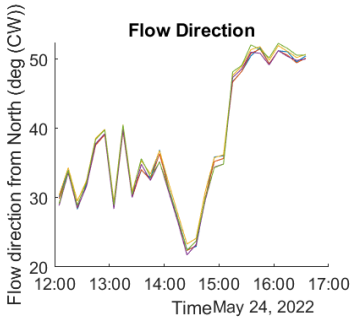

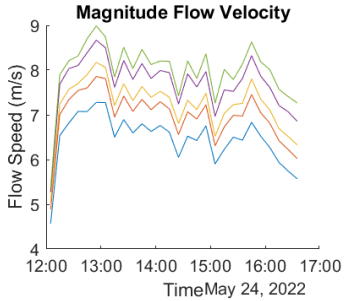

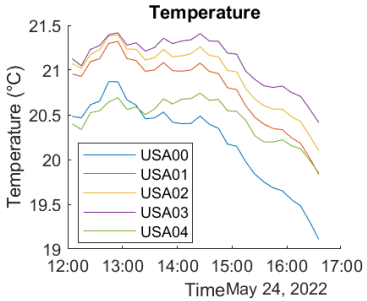

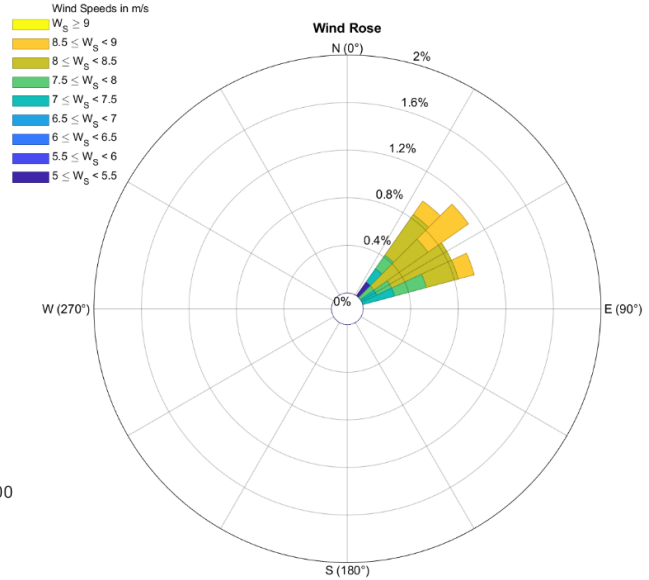

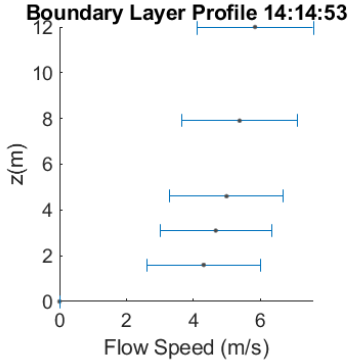

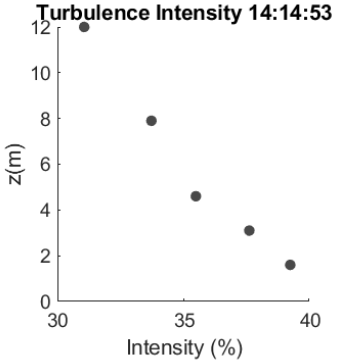

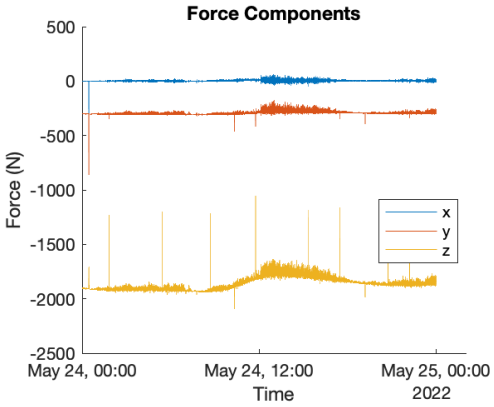

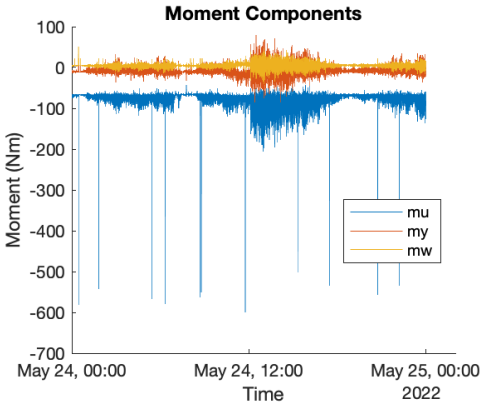

HelioCon gap analysis wind load

Gaps	Approach
WL1: Wind measurement and characterization at heliostat field sites	• Define frequency and resolution of wind measurements for heliostat wind load predictions • Analyse high-frequency DNI and wind data, define site characterization ABL modelling parameters • Wind characterization guidelines (SolarPACES, IEC) for ABL site assessment of wind loads and soiling and publicly available database
WL2: Impact of atmospheric turbulence on dynamic loads and tracking error	• Industry survey, sensitivity analysis of field operational loss per year due to wind • Correlate wind fluctuations with heliostat tracking and slope error • Correlate wind fluctuations with receiver thermal energy capture and flux distribution
WL3: Wind load measurements on heliostats in array configurations	• Characterize loads on arrays of heliostats in wind tunnel and CFD simulations • Analyse and publish wind load coefficients comparing wind tunnel experiments and field measurements
WL8: Design standards for determining heliostat wind load coefficients and safety factors	• Analysis of critical load cases and peak characterization methods for wind loads • Wind load guideline – preliminary draft developed in SolarPACES Task III circulated to HelioCon/industry for review and revisions • Define stow design gust wind speed to reduce uncertainty of heliostat component cost

HelioCon recommended pathway wind load

- Develop methodology and techniques in heliostat field wind testing
  - Synchronous measurement of wind and heliostat slope/tracking error
  - Characterize 3D turbulence length scales and displacement of heliostat components
- Refine wind load design guidelines for single heliostats (SolarPACES Task III)
  - Shielding factors on tandem and array heliostats due to upstream blockage effect
  - Dynamic load multipliers for field-edge and in-field heliostats
  - Define specifications for field zones based on predicted wind loads and opportunities for heliostat mass reduction based on operating angle range and shielding effects
- Develop guidelines for heliostat field site wind assessment
  - Correlate with DNI, soiling, humidity, atmospheric stability
  - Stow design wind speed and partial field stow strategies based on in-field data

University of Adelaide data

- Wind tunnel experiments on scale-model heliostats
  - ABL velocity and turbulence data
  - Load data on single and tandem heliostats
- ABLRF field measurements
  - Wind velocity, turbulence and temperature data
  - Load data on single heliostat
- ASTRI wind load spreadsheet
  https://www.adelaide.edu.au/cet/technologies/heliostat-wind-loads#research-data
- Heliostat wind load design guidelines (SolarPACES)

References

- Emes, M.J., Jafari, A., and Arjomandi, M. (2022), A feasibility study on the application of mesh grids for heliostat wind load reduction, Solar Energy, 240, 121-130. doi:10.1016/j.solener.2022.05.033
- Emes, M., Jafari, A., Pfahl, A., Coventry, J. and Arjomandi, M. (2021), A review of static and dynamic heliostat wind loads, Solar Energy, 225, 60-82. doi: 10.1016/j.solener.2021.07.014
- Jafari, A., Emes, M., Cazzolato, B., Ghanadi, F. and Arjomandi, M. (2021), Wire mesh fences for manipulation of turbulence energy spectrum, Experiments in Fluids, 62(2), 30. doi:10.1007/s00348-021-03133-7
- Emes, M.J., Jafari, A., Coventry, J. and Arjomandi, M. (2020), The influence of atmospheric boundary layer turbulence on the design wind loads and cost of heliostats, Solar Energy, 207, 796-812. doi:10.1016/j.solener.2020.07.022
- Jafari, A., Emes, M., Cazzolato, B., Ghanadi, F. and Arjomandi, M. (2020), Turbulence characteristics in the wake of a heliostat in an atmospheric boundary layer flow, Physics of Fluids, 32(4), 045116. doi:10.1063/5.0005594
- Emes, M.J., Jafari, A., Ghanadi, F. and Arjomandi, M. (2019), Hinge and overturning moments due to unsteady heliostat pressure distributions in a turbulent atmospheric boundary layer, Solar Energy, 193, 604-617. doi:10.1016/j.solener.2019.09.097
- Jafari, A., Ghanadi, F., Emes, M.J., Arjomandi, M. and Cazzolato, B.S. (2019), Measurement of unsteady wind loads in a wind tunnel: scaling of turbulence spectra, Journal of Wind Engineering and Industrial Aerodynamics, 193, 103955. doi:10.1016/j.jweia.2019.103955
- Jafari, A., Ghanadi, F., Arjomandi, M., Emes, M. & Cazzolato, B. (2019). Correlating turbulence intensity and length scale with the unsteady lift force on flat plates in an atmospheric boundary layer flow. Journal of Wind Engineering and Industrial Aerodynamics, 189, 218-230. doi:10.1016/j.jweia.2019.03.029
- Emes, M., Ghanadi, F., Arjomandi, M., & Kelso, R. (2018). Investigation of peak wind loads on tandem heliostats in stow position. Renewable Energy, 121, 548-558. doi:10.1016/j.renene.2018.01.080
- Emes, M., Arjomandi, M., Ghanadi, F., & Kelso, R. (2017). Effect of turbulence characteristics in the atmospheric surface layer on the peak wind loads on heliostats in stow position. Solar Energy, 157, 284-297. doi: 10.1016/j.solener.2017.08.031
- Emes, M., Arjomandi, M., & Nathan, G. (2015). Effect of heliostat design wind speed on the levelised cost of electricity from concentrating solar thermal power tower plants. Solar Energy, 115, 441-451. doi: 10.1016/j.solener.2015.02.047

For a full list of journal and conference publications,
visit www.adelaide.edu.au/cet/technologies/heliostat-wind-loads#list-of-publications

ASTRI Partners

Australian partners

US collaborators

Acknowledgements

- Australian Solar Thermal Research Institute (ASTRI)
- Australian Renewable Energy Agency Grant 1-SRI002
- University of Adelaide
  - Mechanical and electrical workshops
  - Centre for Energy Technology (CET)
  - Institute for Sustainability, Energy and Resources (ISER)
- Conditions Over the Landscape (COtL)
- HelioCon

Students
Callum Rowett
Junhwi Cho
Zeyu Feng
Isaac Miller
Lachlan Carlsson-Forbes
Merritt Boyd
Zoe Ripke
Jeremy Yu

Matthew Emes, University of Adelaide
Email: matthew.emes@adelaide.edu.au | **Phone:** +61883137185
https://www.adelaide.edu.au/cet/technologies/heliostat-wind-loads